Online data and methods supplement

Exacerbation of Adverse Cardiovascular Effects of Aircraft Noise in an Animal Model of Arterial Hypertension

Sebastian Steven[1,2]*, Katie Frenis[1]*, Sanela Kalinovic[1], Miroslava Kvandova[1], Matthias Oelze[1], Johanna Helmstädter[1], Omar Hahad[1], Konstantina Filippou[1], Kamil Kus[3], Chiara Trevisan[4], Klaus-Dieter Schlüter[5], Kerstin Boengler[5], Stefan Chlopicki[3,6], Katrin Frauenknecht[4], Rainer Schulz[5], Mette Sorensen[7,8], Andreas Daiber[1,9]¶, Swenja Kröller-Schön[1]*, Thomas Münzel[1,9]*¶

From the [1] Center for Cardiology, Cardiology I – Laboratory of Molecular Cardiology, University Medical Center of the Johannes Gutenberg-University, Mainz, Germany; [2] Center for Thrombosis and Hemostasis, University Medical Center of the Johannes Gutenberg-University, Mainz, Germany; [3] Jagiellonian Centre for Experimental Therapeutics (JCET); [4] Institute of Neuropathology, University Hospital, Zurich, Switzerland; [5] Department of Physiology, University Gießen, Germany; [6] Chair of Pharmacology, Jagiellonian University, Krakow, Poland; [7] Danish Cancer Society, Copenhagen, Denmark; [8] Department of Natural Science and Environment, Roskilde University, Roskilde, Denmark. [9] German Center for Cardiovascular Research (DZHK), Partner Site Rhine-Main, Mainz.

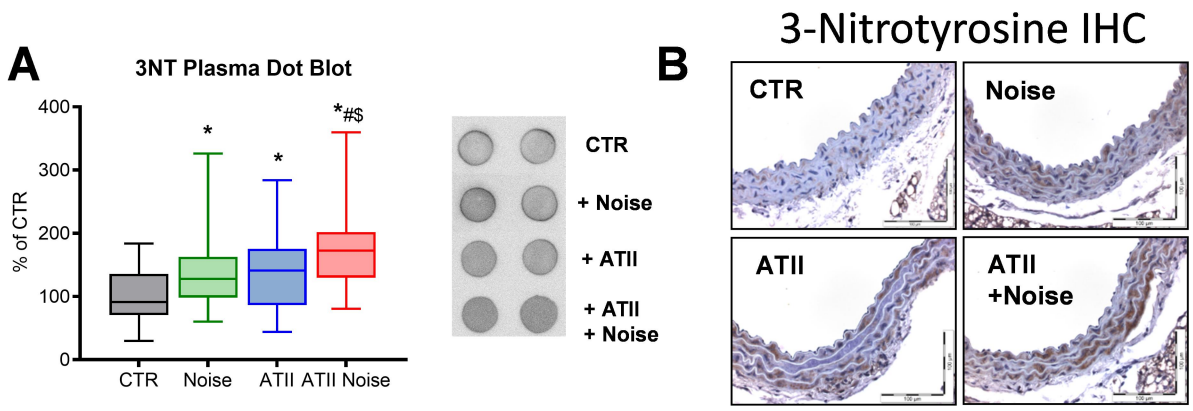

Suppl. Figure S1. 3-nitrotyrosine-positive proteins are increased by both hypertension and noise exposure and further aggravated in the presence of both stressors. (A) Densitometry and representative dot blot of 3-nitrotyrosine (3NT)-positive proteins in plasma denoting nitro-oxidative stress. This may be a consequence of peroxynitrite formation and/or enhanced myeloperoxidase (MPO) expression and higher hydrogen peroxide levels in activated immune cells leading to MPO/H_2O_2/nitrite-catalyzed nitration of tyrosine residues. **(B)** Representative pictures (for at least 4 images per group) of immunohistochemical stainings for 3-nitrotyrosine in aortic sections. Magnification 40x, scale bars represent 50 µm. Data in **(A)** are box and whiskers (with min/max) from at least 8 animals per group. Kruskal-Wallis non-parametric test with Dunn's multiple comparison test; $^{*}P < 0.05$ vs. untreated controls; $^{\#}P < 0.05$ vs. +Noise; $^{\$}P < 0.05$ vs. +ATII.

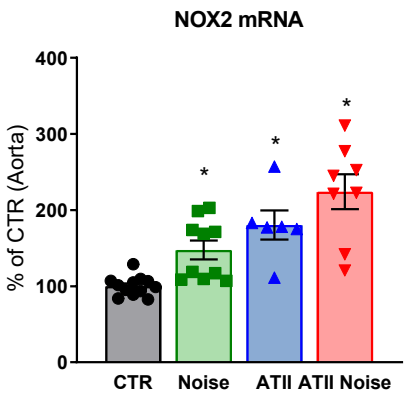

Suppl. Figure S2. *NOX2* mRNA expression in the aorta is increased by both hypertension and noise exposure and by trend aggravated in the presence of both stressors. Expression of *NOX2* was measured by quantitative rtPCR as a source of ROS in response to ATII and noise treatment. Data points are measurements from at least 6 animals; 1-way ANOVA with Tukey's multiple comparison test; *$P < 0.05$ vs. untreated controls.

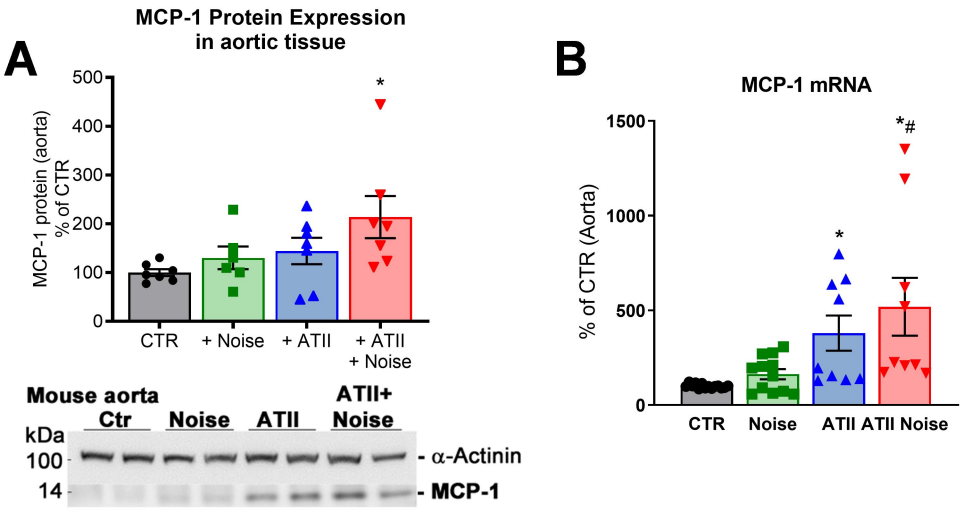

Suppl. Figure S3. Monocyte chemotactic protein-1 (MCP-1) expression in the aorta is aggravated in the presence of combined hypertension and noise exposure. Expression of MCP-1 protein **(A)** was determined by Western blotting (representative Western blots below the densitometry) and of *MCP-1* mRNA **(B)** was measured by quantitative rtPCR as a marker of monocyte activation. Data points are measurements from at least 6 **(A)** and 9 **(B)** animals; 1-way ANOVA with Tukey's multiple comparison test **(A)** and Kruskal-Wallis non-parametric test with Dunn's multiple comparison test **(B)**; $^{*}P < 0.05$ vs. untreated controls; $^{\#}P < 0.05$ vs. +Noise.

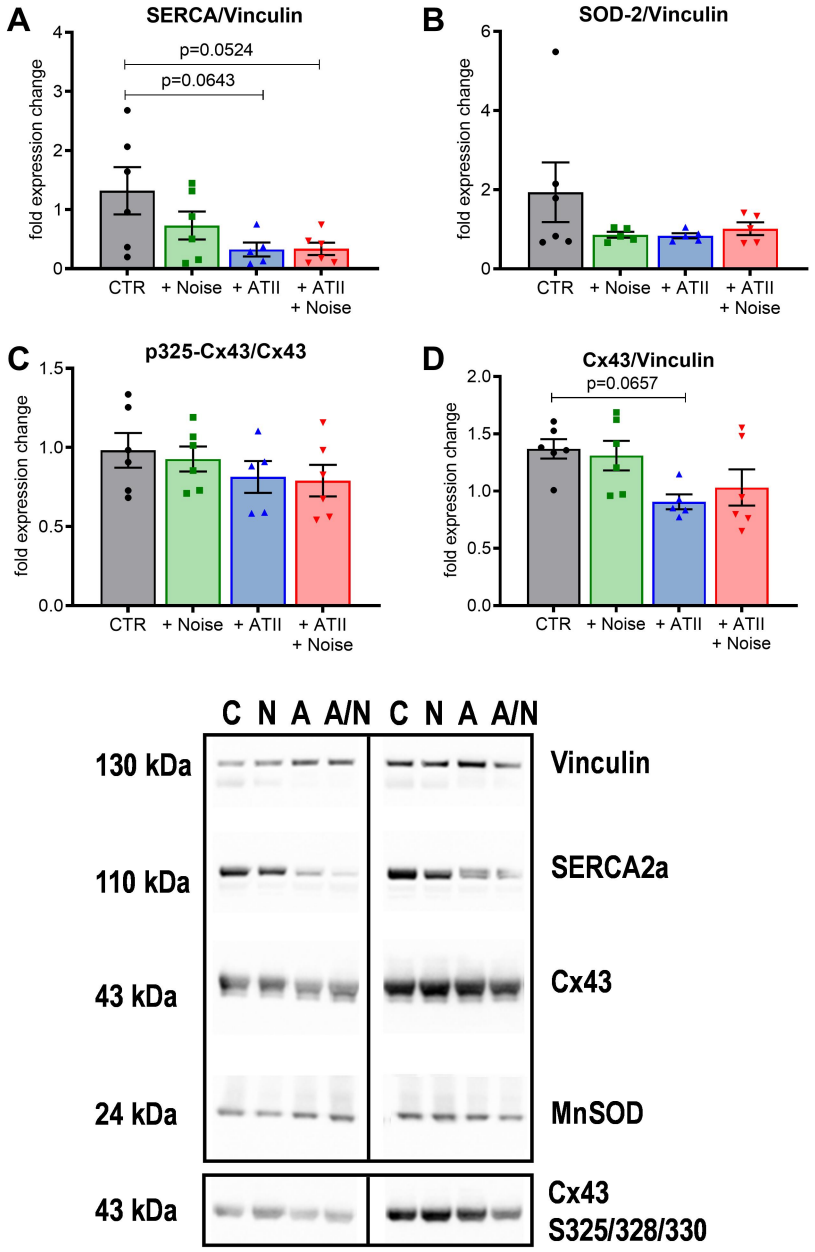

Suppl. Figure S4. Evidence for enhanced structural and antioxidant changes in response to combined hypertension and noise exposure in the heart. (A-D) Expression of proteins of sarco/endoplasmic reticulum Ca^{2+} ATPase (SERCA2a), mitochondrial manganese-superoxide dismutase (MnSOD), phospho-S325/328/330-connexin 43 (pS325-Cx43) and connexin 43 (Cx43) was determined by Western blotting (two representative Western blots are shown below the densitometry). Protein loading was normalized to vinculin. Data points are measurements from at least 5 samples/group (each pooled from 2-4 mice); 1-way ANOVA with Tukey's multiple comparison test.

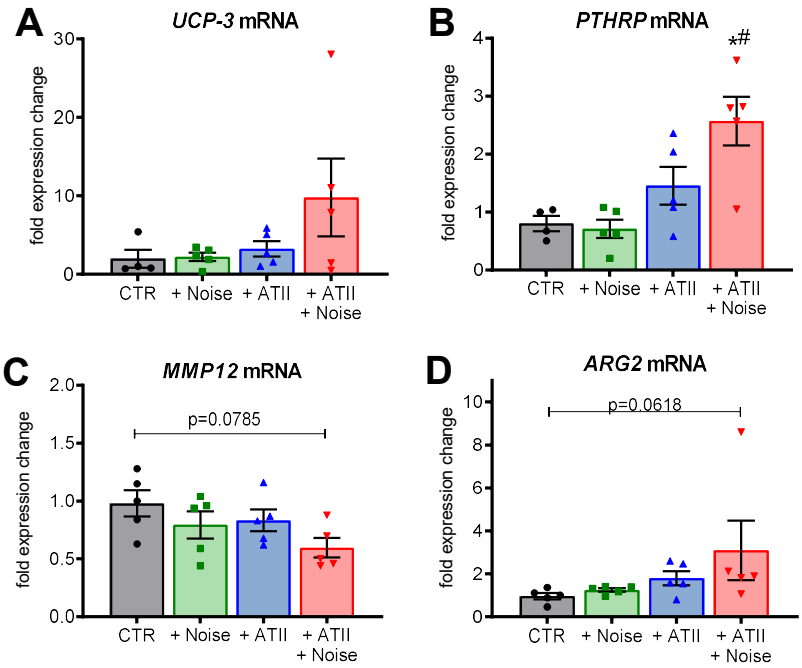

Suppl. Figure S5. Evidence for potentiated structural and metabolic changes in response to combined hypertension and noise exposure in the kidney. (A-E) Expression of genes of uncoupling protein 3 (UCP-3), parathormone-related protein (PTHRP), matrix metalloproteinase 12 (MMP12) and arginase 2 (ARG2) was determined by quantitative rtPCR. Data points are measurements from at least 4 samples/group (each pooled from 2-4 mice); 1-way ANOVA with Tukey's multiple comparison test (**B, C**) and Kruskal-Wallis with Dunn's comparison test (**A, D**); $^{*}P < 0.05$ vs. untreated controls; $^{\#}P < 0.05$ vs. +Noise.

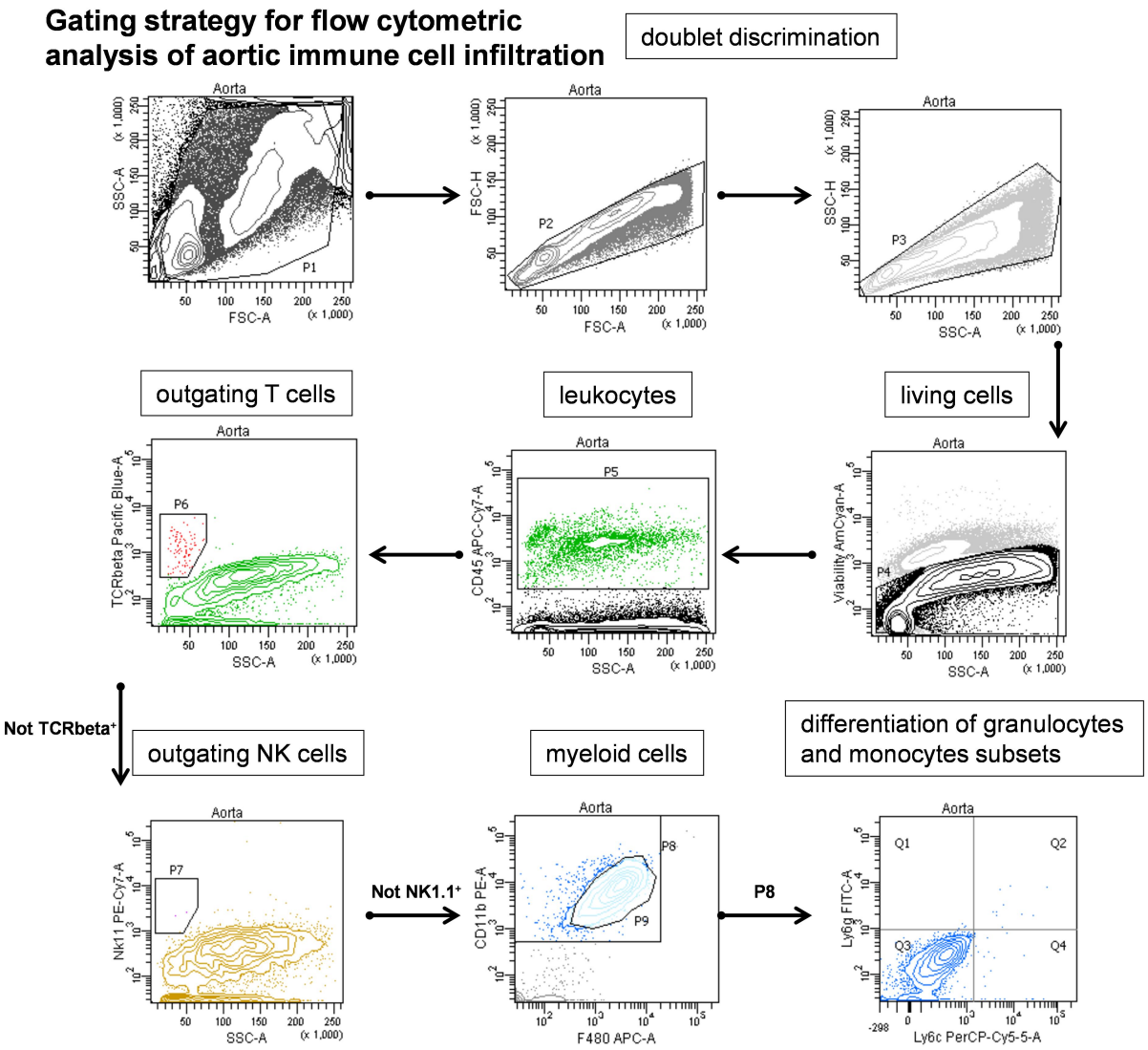

Suppl. Figure S6. Gating strategy for FACS analysis presented in Figure 4 in the main manuscript.

ImageJ-dependent GFAP Analysis:
Measured % of GFAP+ area in the Corpus callosum (% GFAP+ per 400 x 200 micrometer)
GFAP signal (brown before (A) and after color deconvolution (B)) in CC. Area occupied by GFAP (black) in C after adjustment of threshold.

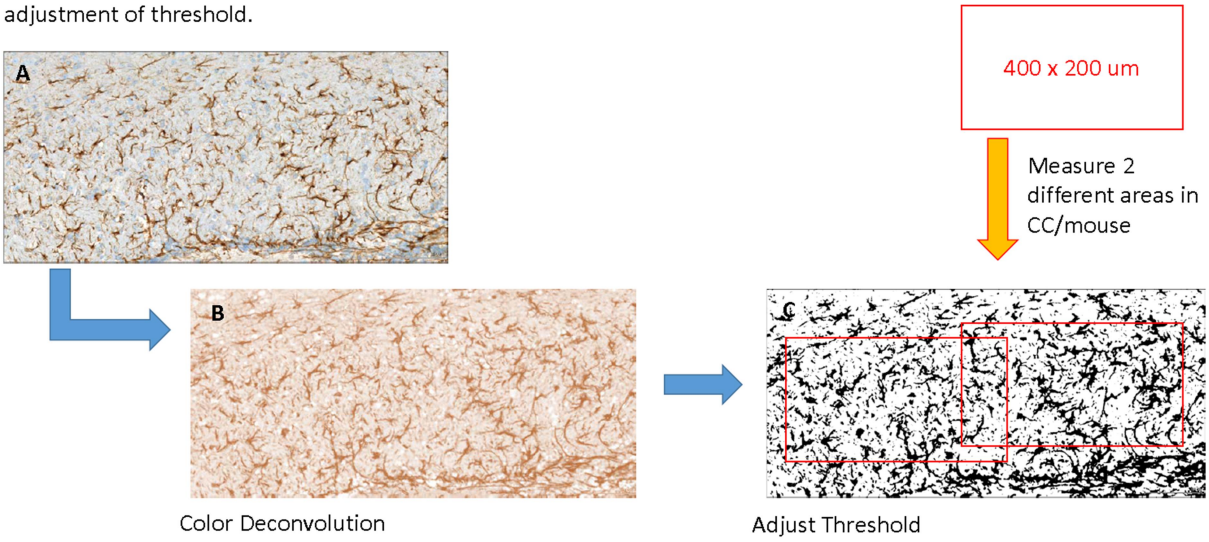

Suppl. Figure S6. Workflow of the GFAP analysis for astrocyte activation in the brain.

2. Extended Materials and Methods

2.7 Isometric tension studies

Aortas were dissected from the animal and cleaned of perivascular fat. 4-mm segments of thoracic aortas were cut and mounted on force transducers within the organ bath chamber. The rings were pre-constricted using prostaglandin $F_{2\alpha}$ to yield approximately 80% of the maximal tone induced by KCl bolus. Concentration-relaxation curves in response to increasing concentrations of acetylcholine (ACh) and nitroglycerine (GTN) were performed as previously described [1, 2].

2.8 Immunohistochemical staining of aortic rings

Aortic segments with adventitia and perivascular fat were fixed in 4% paraformaldehyde and embedded in paraffin. As previously described [3], these samples were cut into sections of 5µm thickness. Samples were deparaffinized and blocked with normal horse blocking solution (Vector) and stained with a primary antibody against either endothelin-1 (Abcam #117757: 1:1000) or 3-nitrotyrosine (Millipore #06-284: 1:200) and biotinylated with a secondary antibody (Thermo Fisher Scientific, Waltham, MA). ABC reagent (Vector) was used for immunochemical detection and DAB reagent (peroxidase substrate kit, Vector) as a substrate. Image ProPlus 7.0 (Media Cybernetics, Rockville, MD) was used to quantify the images as a % of stained area.

2.9 Detection of oxidative stress in plasma, whole blood, cardiac tissue or mitochondria, brain and aorta

Dihydroethidium (1µM)-dependent fluorescence microtopography was used to determine the vascular and cortical ROS formation in cryo-sections of the aorta and prefrontal cortex, as described [4, 5]. To investigate the involvement of eNOS uncoupling in ROS production and endothelial dysfunction, aortic rings were incubated with the NOS inhibitor L-

NAME (0.5mM) and red fluorescence of DHE oxidation products was only quantified in the endothelial cell layer [4-6]. ROS-derived red fluorescence was detected using a Zeiss Axiovert 40 CFL microscope, Zeiss lenses, and Axiocam MRm camera.

Protein tyrosine nitration was detected using a specific antibody for 3-nitrotyrosine (3NT, 1:1,000, Upstate Biotechnology, MA, USA) and lipid peroxidation using a specific antibody for 4-hydroxynonenol (4HNE)-positive proteins (1:5,000, Millipore, MA, USA) in EDTA plasma, as described [7, 8]. 1µl (0.5µg protein) of the EDTA plasma was transferred to each well of a Protran BA85 (0.45µm) nitrocellulose membrane (Schleicher&Schuell, Dassel, Germany) via a Minifold I vacuum Dot-Blot system (Schleicher&Schuell, Dassel, Germany). Each slot was washed twice with 200µl PBS before and after protein transfer. The membrane was dried for 60min at 60°C. Positive bands were detected by enhanced chemiluminescence after incubation with a peroxidase-coupled secondary antibody (goat anti-rabbit and goat anti-mouse, 1:10,000) (Vector Laboratories, CA, USA). All incubation and washing steps were performed according to the manufacturer's instructions. Densitometric quantification of the dots was performed using the Super Signal ECL kit from Thermo Scientific and a ChemiLux Imager (CsX-1400M, Intas, Göttingen, Germany) with Gel-Pro Analyzer software (Media Cybernetics, Bethesda, MD).

Oxidative stress from superoxide was also measured by a modified HPLC-based method to quantify 2-hydroxyethidium levels as previously described [5, 9, 10]. Briefly, tissue of aorta, heart, or frontal cortex was incubated with 50µM DHE for 30min at 37°C in PBS buffer. Tissues were homogenized in 50% acetonitrile/ 50% PBS using a glass homogenizer (heart and brain frontal cortex) or pulverized in a mortar under liquid nitrogen and resuspended in homogenization buffer (aorta), centrifuged and 50µl of the supernatant were subjected to HPLC analysis. The system consisted of a control unit, two pumps, mixer, detectors, column oven, degasser and an autosampler (AS-2057 plus) from Jasco (Groß-

Umstadt, Germany) and a C_{18}-Nucleosil 100-3 (125x4) column from Macherey & Nagel (Düren, Germany). A high pressure gradient was employed with acetonitrile and 50mM citrate buffer pH 2.2 as mobile phases with the following percentages of the organic solvent: 0min, 36%; 7min, 40%; 8-12min, 95%; 13min, 36%. The flow was 1ml/min and DHE was detected by its absorption at 355nm whereas 2-hydroxyethidium was detected by fluorescence (Ex. 480nm/Em. 580nm).

Mitochondrial oxidative stress and superoxide was measured by a modified HPLC-based method to quantify triphenylphosphonium-linked 2-hydroxyethidium (2-OH-mito-E+) levels as previously described [11, 12]. Briefly, cardiac tissues underwent homogenization in HEPES buffer (composition in mM: 50 HEPES, 70 sucrose, 220 mannitol, 1 EGTA (ethylene glycol-bis(β-aminoethyl ether)-N,N,N′,N′-tetraacetic acid), and 0.033 bovine serum albumin) and centrifugation at 1,500g for 10 min at 4°C, followed by another centrifugation step of the supernatant at 2,000g for 5 min (pellets were not used). Next, centrifugation of the supernatant at 20,000g for 20 min was applied, the pellet was collected and a suspension in 1 ml of HEPES buffer was prepared. The suspension was centrifuged again at 20,000g for 20 min, but this time a suspension of the pellet was prepared in 1 ml of Tris buffer (composition in mM: 10 Tris, 340 sucrose, 100 KCl, and 1 EDTA). The resulting mitochondria-enriched suspensions containing 5–10 mg/ml of total protein (according to Lowry assay) were kept at 0°C, were all adjusted to a similar protein content (based on the lowest determined concentration) and were further diluted in 0.5 ml of PBS buffer containing mitoSOX (5 μM) (final protein concentration: 0.1 mg/ml) and then incubated for 15 minutes at 37 °C. After the incubation step 50 v/v% of acetonitrile was added in order to destroy the mitochondrial membrane and extract the mitoSOX oxidation products, samples were subjected to centrifugation and the resulting supernatant was subjected to HPLC analysis (100 μl per sample injection). The HPLC system was purchased from Jasco (Groß-Umstadt, Germany)

with a typical composition (control unit, two pumps for high pressure gradient, high pressure mixer, UV/Vis and fluorescence detectors, and an autosampler (AS-2057 plus with 4 °C cooling device). Generation of gas bubbles from the solvents that can cause an unstable detection baseline were prevented using a degasser unit. . For separation of the product and reactant mixtures, a reversed-phase column was used (C_{18}-Nucleosil 100-3 (125x4), Macherey & Nagel, Düren, Germany). Optimal separation was achieved by application of a high pressure gradient with acetonitrile as the organic/nonpolar component and citrate buffer as the aqueous/polar component (50 mM, pH 2.2) of the mobile phase. The following percentages of the organic solvent were applied: 0 min, 22 %; 10 min, 50 %; 22min, 63 %; 23-25 min, 100 %; 25-27 min, 22%. The flow was 0.5 ml/min and mitoSOX was detected by its absorption at 360 nm whereas mitoE+ and 2-OH-mito-E+ were detected by fluorescence (Ex. 500 nm/Em. 580 nm).

2.10 S-glutathionylation of endothelial nitric oxide synthase by immunoprecipitation

Immunoprecipitation of eNOS and subsequent immunoblotting of the precipitate for S-glutathionylation was performed according to a standard protocol as previously published [13, 14]. M-280 sheep anti-mouse IgG coated beads from Invitrogen (Darmstadt, Germany) were used along with a monoclonal mouse eNOS (Biosciences, USA) antibody. The beads were loaded with the eNOS antibody and cross-linked according to the manufacturer's instructions. Next, aortic homogenates were incubated with the eNOS antibody beads, precipitated with a magnet, washed and transferred to a 7.5% SDS-PAGE gel and treated with a standard non-reducing Western blot procedure using an antibody against S-glutathionylated proteins (mouse monoclonal, 1:1,000, Virogen, Watertown, MA, USA) at a dilution of 1:1,000 under non-reducing conditions. After stripping of the membrane, the bands were immunoblotted for eNOS (mouse monoclonal, 1:1,000, BD Biosciences, USA) for

normalization. Detection and quantification were performed by enhanced chemiluminescence (ECL) with peroxidase conjugated anti–mouse (1:10,000, Vector Lab., Burlingame, CA) secondary antibodies. Densitometric quantification of antibody-specific bands was performed as described above for dot blot analysis.

2.11 Western Blotting Analysis of Other Proteins

Western blotting procedure for aortic tissue was similar to those described in the immunoprecipitation procedure and as reported previously [7, 8]. Protein samples were analyzed for NADPH oxidase 2 ($gp91^{phox}$, mouse monoclonal, 1:1,000, BD Biosciences, USA), phospho-Ser1177-eNOS (rabbit polyclonal, 1:1,000, Cell Signaling, Danvers, MA, USA), phospho-Ser239-VASP (mouse monoclonal, 1.5μg/ml, Millipore, Billierica, MA, USA), heme oxygenase-1 (HO-1, mouse monoclonal, 1:10,000, Abcam, Cambridge, MA, USA), monocyte chemotactic protein-1 (MCP-1, polyclonal, 1:500, Bio-Rad Laboratories GmbH, Germany) and monoclonal mouse α-actinin or polyclonal rabbit β-actin (both 1:2,500, Sigma-Aldrich) for normalization of loading and transfer. Goat anti-mouse and goat anti-rabbit peroxidase-coupled secondary antibodies (1:10,000, Vector Laboratories, CA,USA) were used for the detection of positive bands along with ECL development, as described in the dot blot and immunoprecipitation procedure.

Western blot analysis on mouse cardiac tissue samples was performed as described previously [15]. Mouse total cardiac tissue samples were lysed in 1× Cell lysis buffer (Cell Signaling Technology, Danvers, MA, USA) supplemented with 1× PhosStop and Complete protease inhibitors (Roche, Basel, Switzerland) as well as 1 μM neocuproine. Protein concentration was assessed with Lowry's assay (Thermo Fisher Scientific, Waltham, MA, USA). Protein samples (15 μg/sample) were electrophoretically separated on 10% Bis/Tris gels and were transferred to nitrocellulose membranes. After blocking, membranes were

incubated with the following primary antibodies: anti-Cx43 (1:1000; rabbit polyclonal, C6219, Sigma, St. Louis, MO, USA), anti-Cx43 S325/328/330 (1:2000, mouse monoclonal, kindly provided by Paul D. Lampe, Seattle, USA), anti-sarcoplasmic/endoplasmic reticulum calcium ATPase 2a (SERCA2A; mouse monoclonal, 1:1000; S1314, Sigma), anti-MnSOD (rabbit polyclonal, 1:1000, 06-984, Millipore), anti-Vinculin (mouse monoclonal, 1:1000, V9131, Sigma). After washing and incubation with the respective secondary antibodies (goat-anti rabbit or horse-anti mouse peroxidase-coupled, Cell Signaling), signals were detected with enhanced chemiluminescence (SuperSignal West Femto Chemiluminescent Substrate, Thermo Fisher Scientific, Waltham, MA, USA), visualized by Chemidoc XRS+ gel documentation system (Bio-Rad, Hercules, CA, USA) and analyzed by ScionImage software (Scion Corporation, Frederick, MD, USA).

2.12 Quantitative reverse transcription real-time PCR (qRT-PCR)

Total mRNA from aortic tissue was isolated using the acid guanidinium thiocyanate-phenol-chloroform extraction method. 50ng of total RNA was used for quantitative reverse transcription real-time PCR (qRT-PCR) analysis using QuantiTect Probe RT-PCR kit (Qiagen) as described previously [3, 16]. Primer-probe-mixes purchased from Applied Biosystems (Foster City, CA) were used to analyze the mRNA expression patterns of NADPH oxidase 2 (*NOX-2 Mm00432775_m1*), monocyte chemoattractant protein 1 (*MCP-1, Mm00441243_g1*), cluster of differentiation 68 (*CD68, Mm00839626_m1*), vascular cell adhesion protein 1 (*VCAM-1, Mm00449197_m1*), plasminogen activator inhibitor-1 (*PAI-1, Mm00435860_m1*) and normalized on the *TATA box binding protein* (*TBP*, Mm_00446973_m1) as an internal control. For quantification of the relative mRNA expression the comparative ΔΔCt method was used. Gene expression of target gene in each sample was expressed as the percentage of unexposed wild type.

Total RNA from kidneys was extracted from renal tissue using peqGOLD TriFast (Peqlab, Biotechnologie GmbH, Erlangen, Germany) according to the manufacturer's protocol. To remove genomic DNA contamination, RNA samples were treated with 1 U DNase/µg RNA (Invitrogen, Karlsruhe, Germany) for 15 min at 37°C. One µg of total RNA was used in a 10 µl reaction to synthesize cDNA using Superscript RNaseH Reverse Transcriptase (200 U/µg RNA, Invitrogen, Karlsruhe, Germany). Real-time quantitative PCR was performed using the CFX Connect detection system (Bio-Rad, Munich, Germany) along with the iTaq Universal SYBR Green Real-Time PCR Supermix (Bio-Rad, Munich, Germany). The thermal cycling program consisted of initial denaturation in one cycle of 3 min at 95 °C, followed by 45 cycles of 30 s at 95 °C, 30 s at the individual annealing temperature for each primer, and 30 s at 72 °C. Genes selected for expression analysis: UCP-3 (NM_009464.3), PTHrP (NM_008970.4), MMP12 (NM_008605.3) and ARG2 (NM_009705.3). Isolation and measurement was previously described [17]. Quantification was performed as described before [18]. Data was normalized to hypoxanthine phosphoribosyl transferase (HPRT).

2.13 Determination of nitrate and nitrite concentration in plasma

The concentrations of nitrite and nitrate were measured by ENO-20 NOx Analyzer (Eicom Corporation, Tokyo, Japan), based on the liquid chromatography method with post column derivatization with Griess reagent [19]. The plasma samples were precipitated with methanol at the ratio of 1:1 (v/v) and subsequently centrifuged at 10,000 x g for 10min. 10µL of supernatant was injected into the HPLC system. Nitrite and nitrate were separated on a NO-PAK column (4.6µm x 50mm; Eicom). Nitrate was reduced to nitrite by a cadmium-copper column (NO-RED; Eicom). Nitrite was detected based on the Griess reaction, with sulfanilamide and naphthylethylenediamine (both from NO-EBP, Eicom) forming a purple

diazo compound (tR= 4.9min for nitrite and 7.8min for nitrate) with UV/Vis detection at 540nm.

2.14 Flow cytometry of aortic tissue lysates

Flow cytometry of aortas was performed like described previously [20, 21]. Briefly, aortic vessels were cleaned of fatty tissue, minced and digested with liberase™ (1mg/ml, Roche, Basel, Switzerland) for 30min at 37°C. By passing the lysed aortic fragments through a cell strainer (70µm), a single-cell suspension was obtained. Single-cell suspensions were treated with Fc-block (anti-CD16/CD32), washed and surface stained with CD45 APC-efluor 780 (#47-0451-82, 2µg/mL), NK1.1 PE-Cy7 (#25-5941-81, 2µg/mL), F4/80 APC (#17-4801-82, 4µg/mL) from eBioscience (San Diego, CA) and TCR-β V450 (#560706, 2µg/mL), CD11b PE (#553311, 2µg/mL), Ly6G FITC (#551460, 5µg/mL), Ly6C PerCP-Cy.5.5 (#560525, 2µg/mL) from BD Biosciences (San Diego, CA). Dead cells were excluded by staining with Fixable Viability Dye eFluor506 (#65-0866-14, 1:1000, eBioscience, San Diego, CA). Based on a live gate, events were acquired and analyzed using a BD FACS CANTO II flow cytometer (Becton Dickinson, Franklin Lakes, NJ) and FACSDiva software (Becton Dickinson, Franklin Lakes, NJ), respectively.

Extended References

[1] T. Munzel, A. Giaid, S. Kurz, D.J. Stewart, D.G. Harrison. Evidence for a role of endothelin 1 and protein kinase C in nitroglycerin tolerance. Proc Natl Acad Sci 92 (1995) 5244-5248.

[2] M. Oelze, M. Knorr, S. Kroller-Schon, S. Kossmann, A. Gottschlich, R. Rummler, A. Schuff, S. Daub, C. Doppler, H. Kleinert, T. Gori, A. Daiber, T. Munzel. Chronic therapy with isosorbide-5-mononitrate causes endothelial dysfunction, oxidative stress, and a marked increase in vascular endothelin-1 expression. Eur Heart J 34 (2013) 3206-3216, https://doi.org/10.1093/eurheartj/ehs100.

[3] M. Oelze, S. Kroller-Schon, P. Welschof, T. Jansen, M. Hausding, Y. Mikhed, P. Stamm, M. Mader, E. Zinssius, S. Agdauletova, A. Gottschlich, S. Steven, E. Schulz, S.P. Bottari, E. Mayoux, T. Munzel, A. Daiber. The sodium-glucose co-transporter 2 inhibitor empagliflozin improves diabetes-induced vascular dysfunction in the streptozotocin diabetes rat model by interfering with oxidative stress and glucotoxicity. PLoS One 9 (2014) e112394, https://doi.org/10.1371/journal.pone.0112394.

[4] M. Oelze, A. Daiber, R.P. Brandes, M. Hortmann, P. Wenzel, U. Hink, E. Schulz, H. Mollnau, A. von Sandersleben, A.L. Kleschyov, A. Mulsch, H. Li, U. Forstermann, T. Munzel. Nebivolol inhibits superoxide formation by NADPH oxidase and endothelial dysfunction in angiotensin II-treated rats. Hypertension 48 (2006) 677-684, https://doi.org/10.1161/01.HYP.0000239207.82326.29.

[5] P. Wenzel, E. Schulz, M. Oelze, J. Muller, S. Schuhmacher, M.S. Alhamdani, J. Debrezion, M. Hortmann, K. Reifenberg, I. Fleming, T. Munzel, A. Daiber. AT1-receptor blockade by telmisartan upregulates GTP-cyclohydrolase I and protects eNOS in diabetic rats. Free Radic Biol Med 45 (2008) 619-626, https://doi.org/10.1016/j.freeradbiomed.2008.05.009.

[6] M. Oelze, M. Knorr, S. Schuhmacher, T. Heeren, C. Otto, E. Schulz, K. Reifenberg, P. Wenzel, T. Munzel, A. Daiber. Vascular dysfunction in streptozotocin-induced experimental diabetes strictly depends on insulin deficiency. J Vasc Res 48 (2011) 275-284, https://doi.org/10.1159/000320627.

[7] T. Munzel, A. Daiber, S. Steven, L.P. Tran, E. Ullmann, S. Kossmann, F.P. Schmidt, M. Oelze, N. Xia, H. Li, A. Pinto, P. Wild, K. Pies, E.R. Schmidt, S. Rapp, S. Kroller-Schon. Effects of noise on vascular function, oxidative stress, and inflammation: mechanistic insight from studies in mice. Eur Heart J 38 (2017) 2838-2849, https://doi.org/10.1093/eurheartj/ehx081.

[8] S. Kroller-Schon, A. Daiber, S. Steven, M. Oelze, K. Frenis, S. Kalinovic, A. Heimann, F.P. Schmidt, A. Pinto, M. Kvandova, K. Vujacic-Mirski, K. Filippou, M. Dudek, M. Bosmann, M. Klein, T. Bopp, O. Hahad, P.S. Wild, K. Frauenknecht, A. Methner, E.R. Schmidt, S. Rapp, H. Mollnau, T. Munzel. Crucial role for Nox2 and sleep deprivation in aircraft noise-induced vascular and cerebral oxidative stress, inflammation, and gene regulation. Eur Heart J 39 (2018) 3528-3539, https://doi.org/10.1093/eurheartj/ehy333.

[9] H. Zhao, J. Joseph, H.M. Fales, E.A. Sokoloski, R.L. Levine, J. Vasquez-Vivar, B. Kalyanaraman. Detection and characterization of the product of hydroethidine and intracellular superoxide by HPLC and limitations of fluorescence. Proc Natl Acad Sci U S A 102 (2005) 5727-5732.

[10] P. Wenzel, H. Mollnau, M. Oelze, E. Schulz, J.M. Wickramanayake, J. Muller, S. Schuhmacher, M. Hortmann, S. Baldus, T. Gori, R.P. Brandes, T. Munzel, A. Daiber. First evidence for a crosstalk between mitochondrial and NADPH oxidase-derived reactive oxygen species in nitroglycerin-triggered vascular dysfunction. Antioxid Redox Signal 10 (2008) 1435-1447, https://doi.org/10.1089/ars.2007.1969.

[11] J. Zielonka, S. Srinivasan, M. Hardy, O. Ouari, M. Lopez, J. Vasquez-Vivar, N.G. Avadhani, B. Kalyanaraman. Cytochrome c-mediated oxidation of hydroethidine and mito-hydroethidine in mitochondria: identification of homo- and heterodimers. Free Radic Biol Med 44 (2008) 835-846, https://doi.org/10.1016/j.freeradbiomed.2007.11.013.

[12] S. Kalinovic, M. Oelze, S. Kroller-Schon, S. Steven, K. Vujacic-Mirski, M. Kvandova, I. Schmal, A. Al Zuabi, T. Munzel, A. Daiber. Comparison of Mitochondrial Superoxide Detection Ex Vivo/In Vivo by mitoSOX HPLC Method with Classical Assays in Three Different Animal Models of Oxidative Stress. Antioxidants 8 (2019), https://doi.org/10.3390/antiox8110514.

[13] S. Schuhmacher, M. Oelze, F. Bollmann, H. Kleinert, C. Otto, T. Heeren, S. Steven, M. Hausding, M. Knorr, A. Pautz, K. Reifenberg, E. Schulz, T. Gori, P. Wenzel, T. Munzel, A. Daiber. Vascular dysfunction in experimental diabetes is improved by pentaerithrityl tetranitrate but not isosorbide-5-mononitrate therapy. Diabetes 60 (2011) 2608-2616, https://doi.org/10.2337/db10-1395.

[14] S. Kroller-Schon, S. Steven, S. Kossmann, A. Scholz, S. Daub, M. Oelze, N. Xia, M. Hausding, Y. Mikhed, E. Zinssius, M. Mader, P. Stamm, N. Treiber, K. Scharffetter-Kochanek, H. Li, E. Schulz, P. Wenzel, T. Munzel, A. Daiber. Molecular mechanisms of the crosstalk between mitochondria and NADPH oxidase through reactive oxygen species-studies in white blood cells and in animal models. Antioxid Redox Signal 20 (2014) 247-266, https://doi.org/10.1089/ars.2012.4953.

[15] K. Boengler, P. Bencsik, J. Paloczi, K. Kiss, M. Pipicz, J. Pipis, P. Ferdinandy, K.D. Schluter, R. Schulz. Lack of Contribution of p66shc and Its Mitochondrial Translocation to Ischemia-Reperfusion Injury and Cardioprotection by Ischemic Preconditioning. Frontiers in physiology 8 (2017) 733, https://doi.org/10.3389/fphys.2017.00733.

[16] M. Hausding, K. Jurk, S. Daub, S. Kroller-Schon, J. Stein, M. Schwenk, M. Oelze, Y. Mikhed, J.G. Kerahrodi, S. Kossmann, T. Jansen, E. Schulz, P. Wenzel, A.B. Reske-Kunz, C. Becker, T. Munzel, S. Grabbe, A. Daiber. CD40L contributes to angiotensin II-induced pro-thrombotic state, vascular inflammation, oxidative stress and endothelial dysfunction. Basic Res Cardiol 108 (2013) 386, https://doi.org/10.1007/s00395-013-0386-5.

[17] R. Schreckenberg, A.M. Horn, R.M. da Costa Rebelo, S. Simsekyilmaz, B. Niemann, L. Li, S. Rohrbach, K.D. Schluter. Effects of 6-months' Exercise on Cardiac Function, Structure and Metabolism in Female Hypertensive Rats-The Decisive Role of Lysyl Oxidase and Collagen III. Frontiers in physiology 8 (2017) 556, https://doi.org/10.3389/fphys.2017.00556.

[18] K.J. Livak, T.D. Schmittgen. Analysis of relative gene expression data using real-time quantitative PCR and the 2(-Delta Delta C(T)) Method. Methods 25 (2001) 402-408, https://doi.org/10.1006/meth.2001.1262.

[19] K. Kus, M. Walczak, E. Maslak, A. Zakrzewska, A. Gonciarz-Dytman, P. Zabielski, B. Sitek, K. Wandzel, A. Kij, A. Chabowski, R.J. Holland, J.E. Saavedra, L.K. Keefer, S. Chlopicki. Hepatoselective Nitric Oxide (NO) Donors, V-PYRRO/NO and V-PROLI/NO, in Nonalcoholic Fatty Liver Disease: A Comparison of Antisteatotic Effects with the Biotransformation and Pharmacokinetics. Drug Metab Dispos 43 (2015) 1028-1036, https://doi.org/10.1124/dmd.115.063388.

[20] P. Wenzel, M. Knorr, S. Kossmann, J. Stratmann, M. Hausding, S. Schuhmacher, S.H. Karbach, M. Schwenk, N. Yogev, E. Schulz, M. Oelze, S. Grabbe, H. Jonuleit, C. Becker, A. Daiber, A. Waisman, T. Munzel. Lysozyme M-positive monocytes mediate

angiotensin II-induced arterial hypertension and vascular dysfunction. Circulation 124 (2011) 1370-1381, https://doi.org/10.1161/CIRCULATIONAHA.111.034470.

[21] S. Kossmann, M. Schwenk, M. Hausding, S.H. Karbach, M.I. Schmidgen, M. Brandt, M. Knorr, H. Hu, S. Kroller-Schon, T. Schonfelder, S. Grabbe, M. Oelze, A. Daiber, T. Munzel, C. Becker, P. Wenzel. Angiotensin II-induced vascular dysfunction depends on interferon-gamma-driven immune cell recruitment and mutual activation of monocytes and NK-cells. Arterioscler Thromb Vasc Biol 33 (2013) 1313-1319, https://doi.org/10.1161/ATVBAHA.113.301437.